Zeng Zhao-Cheng (Orcid ID: 0000-0002-0008-6508)
Natraj Vijay (Orcid ID: 0000-0003-3154-9429)
Xu Feng (Orcid ID: 0000-0001-5155-9478)
Shia Run-Lie (Orcid ID: 0000-0003-1911-3120)
Kort Eric, A. (Orcid ID: 0000-0003-4940-7541)
Toon Geoffrey, C (Orcid ID: 0000-0003-4174-7541)
Sander Stanley (Orcid ID: 0000-0003-1424-3620)

Constraining Aerosol Vertical Profile in the Boundary Layer Using Hyperspectral Measurements of Oxygen Absorption

Zhao-Cheng Zeng[1], Vijay Natraj[2], Feng Xu[2], Thomas J. Pongetti[2], Run-Lie Shia[1], Eric A. Kort[3], Geoffrey C. Toon[2], Stanley P. Sander[2], and Yuk L. Yung[1,2]

[1] Division of Geological and Planetary Sciences, California Institute of Technology
[2] Jet Propulsion Laboratory, California Institute of Technology
[3] Department of Climate and Space Sciences and Engineering, University of Michigan

Corresponding author: Zhao-Cheng Zeng (zcz@gps.caltech.edu)

Key Points:

- A method is developed to constrain aerosol vertical profiles in the boundary layer using hyperspectral measurements of oxygen absorption
- The method is tested using hyperspectral measurement of reflected solar radiation from a mountain-top instrument to infer aerosol profiles
- The method can potentially be applied to satellite observations to constrain aerosol vertical structure on a global scale

This is the author manuscript accepted for publication and has undergone full peer review but has not been through the copyediting, typesetting, pagination and proofreading process, which may lead to differences between this version and the Version of Record. Please cite this article as doi: 10.1029/2018GL079286

Abstract

This study attempts to infer aerosol vertical structure in the urban boundary layer using passive hyperspectral measurements. A spectral sorting technique is developed to retrieve total aerosol optical depth (AOD) and effective aerosol layer height (ALH) from hyperspectral measurements in the 1.27 μm oxygen absorption band by the mountain-top CLARS-FTS instrument (a.s.l. 1673 meters) overlooking the LA basin. Comparison to AOD measurements from AERONET and aerosol backscatter profile measurements from a Mini MicroPulse Lidar (MiniMPL) shows agreement, with coefficients of determination (r^2) of 0.74 for AOD and 0.57 for effective ALH. On average, the AOD retrieval has an error of 24.9% and root mean square error (RMSE) of 0.013 while the effective ALH retrieval has an error of 7.8% and RMSE of 67.01 m. The proposed method can potentially be applied to existing and future satellite missions with hyperspectral oxygen measurements to constrain aerosol vertical distribution on a global scale.

Plain Language Summary

Satellite and ground-based measurements have enabled accurate and continuous monitoring of total aerosol loading. However, these measurements provide little or no information on the vertical distribution of aerosols. In particular, there is poor measurement of aerosols in the planetary boundary layer, the part of the atmosphere closest to the surface. In this study, we

develop an algorithm to retrieve the vertical structure of aerosols in the boundary layer using remote sensing observations of oxygen absorption with high spectral resolution. The algorithm is applied to infer the vertical profile of air pollutants in the Los Angeles basin using measurements made by a mountaintop instrument overlooking the basin. The proposed retrieval algorithm can potentially be applied to existing and future satellite missions with hyperspectral oxygen measurements to constrain the aerosol vertical distribution on a global scale. This important piece of information on aerosol vertical structure will potentially address several key priorities in the 2017 US National Research Council Earth Science Decadal Survey, from forecasting air pollution in cities, quantifying the aerosol impact on Earth's climate, and reducing biases in greenhouse gas retrievals.

1. Introduction

Information about the global abundance, properties and height distribution of aerosols is needed to quantify their influence on the Earth's climate and to better validate climate models, (IPCC, 2013). In addition, the health effects from pollution are the largest environmental risk (Liu and Diner, 2016). Aerosols also affect greenhouse gas retrievals from space by influencing the path of atmospheric radiation (see, e.g., Kuang et al. 2002; Butz et al., 2009; O'Dell et al., 2012). Aerosols also affect fluorescence retrievals performed in O_2 absorption bands (Frankenberg et al., 2011). Aerosols, including those that contribute to poor air quality, are produced primarily within the planetary boundary layer (PBL), which is the bottom layer of the atmosphere and couples the Earth's surface and the atmosphere above. However, this near-surface layer is relatively poorly modeled, including the air pollutants trapped within this mixing layer. Improving our understanding of the PBL processes is critical to model the coupling mechanisms between the atmosphere and land in the integrated Earth system. Moreover, more accurate representation of the PBL processes related to aerosol horizontal and vertical distributions and composition can

improve modeling of cloud formation and atmospheric radiative transfer (Zarzycki and Bond, 2010).

Column measurements of aerosol optical depth (AOD) have been accurately and continuously observed by satellites such as MODIS (Kahn et al., 2007) and MISR (Diner et al., 1998) and by ground-based measurements from AERONET (Holben et al., 1998). These measurements provide little or no information on the vertical distribution of aerosols. Lidar measurements (Winker et al., 2009) have proven helpful in providing information that locates aerosol layers using active remote sensing. However, lidar instruments have a narrow swath and it is therefore very difficult to obtain a global coverage. It has long been recognized that passive remote sensing using absorption spectroscopy of molecular oxygen has the potential for aerosol vertical profiling (Yamamoto and Wark, 1961; Hou et al., 2017). Absorption in the center of strong O_2 lines is saturated, such that any radiance measured in these regions must originate from scattering in the upper part of the atmosphere. In weak lines light can penetrate to lower atmospheric layers, allowing for the quantification of aerosols and other scatterers near the surface. This passive technique has been used to study cloud top height and cloud thickness (Yamamoto and Wark, 1961; O'Brien and Mitchell, 1992; Heidinger and Stephens, 2000; Richardson et al., 2017), and to investigate its potential for aerosol profiling using theoretical studies (Timofeyev et al., 1995; Gabella et al., 1999; Davis et al. 2017; Colosimo et al., 2017; Geddes and Bosch, 2015; Hollstein and Fischer, 2014) and broadband oxygen measurements from SCIAMACHY (Sanghavi et al., 2015), DSCOVR (Xu et al., 2017), POLDER and MERIS (Dubuisson et al., 2009). In addition, satellite and airborne measurements in the ultraviolet may have the potential to retrieve the absorbing aerosol layer height (Torres et al., 1998; Xu et al., 2017). Model simulations have shown that spectrally resolved (hereafter referred to as hyperspectral) measurements in O_2 absorption bands have, in principle, sufficient information content for quantifying the aerosol vertical distribution and its optical and microphysical properties (Hou et al., 2017). However, very limited progress has been made using real measurements. Aerosol profiling within the boundary layer is even more challenging because

resolving the aerosol profile at sub-kilometer scales requires accurate hyperspectral measurements, good knowledge of aerosol optical properties and compositions and correct characterization of surface reflection.

In this study, an algorithm based on a spectral sorting technique is proposed to retrieve the total AOD and the effective aerosol layer height (ALH) in the boundary layer using hyperspectral measurements in the oxygen band centered at 1.27 μm. The algorithm is applied to measurements made by the Fourier Transform Spectrometer at the California Laboratory for Atmospheric Remote Sensing (CLARS-FTS), located on the top of Mt. Wilson (a.s.l. 1673 meters) overlooking the LA basin.

2. Data

2.1 Observations from CLARS

The CLARS-FTS instrument is located on the top of Mt. Wilson (a.s.l. 1673 meters) in the LA basin and offers continuous high-resolution spectral measurements in the near infrared (NIR) to shortwave infrared (SWIR) spectral region (effectively from 4000 cm^{-1} to 12000 cm^{-1}),

including the oxygen $^1\Delta$ band at 1.27 μm. As shown in **Figure S1**, CLARS has two modes of operation: the Spectralon Viewing Observation mode (SVO), which quantifies the solar irradiance by measuring reflected sunlight from a Spectralon plate located immediately below the FTS telescope, and the Los Angeles Basin Survey mode (LABS), which measures reflected sunlight from surface targets in the basin. In this study, we focus on the West Pasadena surface target, as illustrated in **Figure S2(a)**. The CLARS observation geometry makes the measurements not only highly sensitive to the atmospheric composition but also very susceptible to influence by aerosol scattering and absorption due to the long light path across the boundary layer. The CLARS measurements mimic to a certain extent the off-nadir viewing of an instrument in geostationary orbit with hourly viewing capability. Details concerning the CLARS-FTS design, operation and calibration can be found in Fu et al. (2014), Wong et al. (2015, 2016) and Zeng et al. (2017). High and low clouds are filtered from the CLARS data using the oxygen ratio approach (Wong et al., 2015). This study does not require the CLARS spectra to be radiometrically calibrated since only the CLARS level reflectance (the ratio of the LABS and SVO radiances) is used, as shown in **Figure S1(b)**.

2.2 AERONET AOD measurements

The AERONET site at Caltech makes measurements of total AOD, from which aerosol optical properties including single scattering albedo (SSA) and phase function can be retrieved. **Text S1** introduces the estimation of AOD value in the O_2 $^1\Delta$ band at 1.27 μm using the Ångström exponent law. **Figure S3** shows the seasonal histograms of AOD, SSA, and asymmetry parameter from the aerosol scattering phase function obtained from AERONET-Caltech from 2011 to 2017.

2.3 MiniMPL aerosol backscatter measurements

The MiniMPL instrument, located at Caltech, measures the aerosol backscattering at different altitudes by emitting 532 nm laser light and determining the distance to scattering events using the time of light travel (Ware et al., 2016). The raw event count reported by the MiniMPL at a

vertical resolution of 30 m must be calibrated and normalized in order to arrive at the quantity of interest, *viz.* normalized relative backscatter (NRB), which is approximately proportional to the concentration of scatterers at a given distance above the instrument. Measurement data from 2012 to 2014 are used in this study. **Figure 1(a)** shows the seasonal mean and variabilities of vertical profiles of NRB at 2:00 pm. The aerosol layer in the summer is relatively high mainly due to the expanded boundary layer. The calculation of effective ALH is introduced in **Text S2**. As a measure of the aerosol vertical expansion, the geometric thickness of the aerosol layer in this study is defined as the ratio of the integrated total NRB over all different levels to the maximum NRB. It is physically correlated with effective ALH driven by the expansion and collapse of the PBL. As shown in **Figure 1(b)**, these two data have a significant correlation in the boundary layer (r^2 = 0.67). This correlation can be used to construct the vertical profile together with retrieved total AOD and effective ALH in the boundary layer.

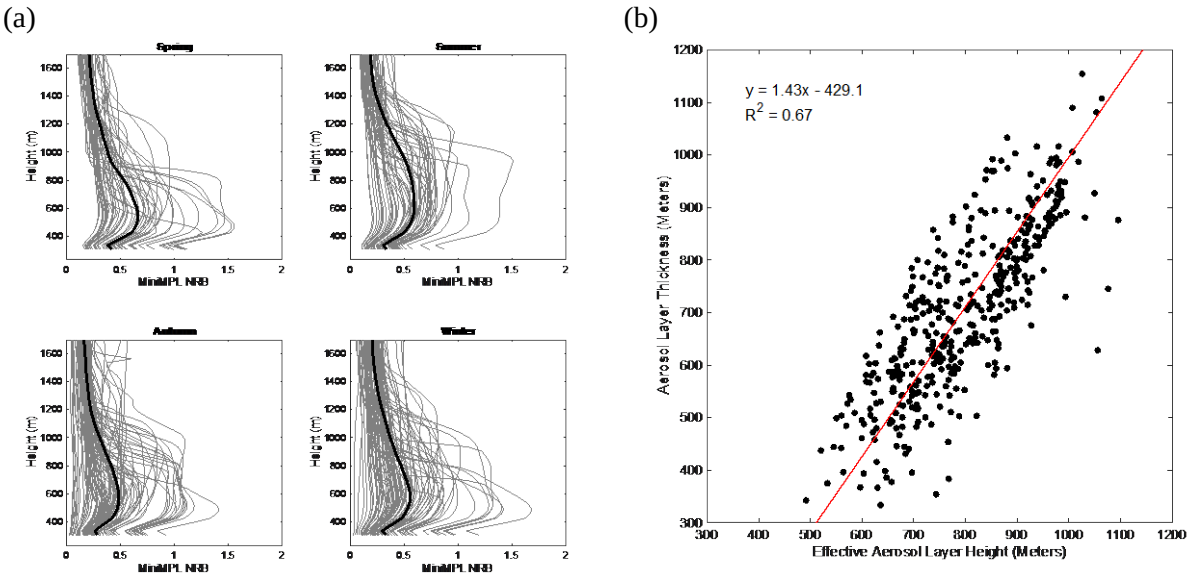

Figure 1. (a) Seasonal mean and variabilities of vertical profiles of normalized relative backscatter (NRB) at 2:00 pm measured by MiniMPL located at Caltech. The grey lines are all the available measurements from 2012 to 2014, and the bold black lines are the seasonal means. (b) Correlation between effective aerosol layer height and geometric thickness calculated using

the MiniMPL measurements as shown in (a). The two parameters have a significant correlation ($r^2 = 0.67$).

3. Retrieval of aerosol vertical profile

3.1 Sensitivity study and spectral sorting

To understand the impact of aerosol vertical structure on the radiance observed by CLARS, a forward radiative transfer (RT) simulation is performed using the 2S-ESS RT model (Spurr and Natraj, 2011; Zhang et al., 2015; Zeng et al., 2017). The RT model settings are described in **Text S3**. **Figure 2(a)** shows the aerosol layer structures in the RT model. Five aerosol layers are constructed by equally dividing the height from the surface (292 meters for West Pasadena surface target) to the CLARS elevation (1673 meters). The layers are centered at 430, 706, 983, 1259, and 1535 meters, respectively, with a layer vertical thickness of 276 meters. The selection of five layers is limited by measurement uncertainty from CLARS to build up a look up table for ALH retrievals as described in Section 3.2. Five scenarios are simulated by adding the same amount of aerosol loading but in different layers. **Figure 2(b)** shows the simulated CLARS reflectance in the 1.27 μm band for the five scenarios as well as the clear sky scenario. Since the aerosol has a higher reflectivity than the surface, the observed radiances are significantly larger for the five aerosol cases than the clear sky case. These simulations use the solar geometries at 14:00 LT in September 2013 and co-located aerosol optical properties (SSA and phase function) from AERONET. We can see that, for the different scenarios, the radiance values are similar in the continuum but different within the absorption bands, with stronger absorption when the aerosol layer is placed at a lower altitude. These differences are even more obvious when we sort the radiance, as shown in **Figure 2(c)**. This is done by sorting the reflectance from the clear sky spectrum and then applying the same order to other scenarios with aerosol scattering. Using this approach, strong, medium and weak lines appear on the left, middle and right sections of each curve, respectively. There are at least two pieces of information directly available from the spectral comparison: (1) the continuum level constrains the total AOD since O_2 absorption is

weak and therefore the radiance is directly related to aerosol loading along the light path given surface albedo is unchanged; (2) the reflected radiance in the intermediate absorption lines, as shown in **Figures 2(c)** and **(d)**, exhibits large differences among the different aerosol scenarios and therefore its variability constrains ALH. The strongest absorption lines are not used in order to avoid the associated large uncertainty in the measurement (due to saturation effects). The small wiggles in the sorted radiance are caused by the fact that wavelength dependence of the oxygen absorption coefficients is different at different altitudes, which in turn is because they vary differently with pressure and temperature. The physical basis of using oxygen to study aerosol scattering is that atmospheric aerosols scatter photons back to space and therefore reduce the chance of the photons being absorbed by the oxygen, which is almost uniformly distributed in the atmosphere. Photons scattered by higher aerosol layers undergo shorter absorption paths, thereby reducing the O_2 absorption depths.

From this sensitivity study, we can see that the observed hyperspectral radiance in the oxygen band has strong sensitivities to both aerosol loading and aerosol vertical structure within the boundary layer. The spectral sorting technique provides a straightforward way to extract the information on aerosol loading and its vertical structure from the observed radiance.

3.2 AOD and ALH retrievals

The retrieval is implemented in two steps. First, the total AOD is retrieved by constructing a lookup table with different aerosol loadings, as shown in **Figures S5(a)** and **(b)**, for the purpose of fitting the observed and simulated radiances in the continuum. Subsequently, another lookup table is built by placing aerosols in different layers and comparing the simulated spectra with observations, as shown in **Figure 2(e)**. The measurements are relatively noisy compared to model simulations, probably because the model simplifies some physical processes that are otherwise hard to capture. It is evident from the measurements that the effective height of the aerosol layer lies between the first (ALH: 430 meters) and second (ALH: 706 meters) layers, while being closer to the latter. A quantitative comparison between measurements and

simulations is needed to get the exact effective ALH. To minimize the impact of data noise on the comparison, we fit the sorted spectra to quantify the spectral shape, as described in **Text S4**. Different metrics can be used to quantify the difference in reflectance between model simulations and measurements. Here, we use the mean value of reflectance over this intermediate absorption window calculated by averaging all CLARS level reflectance values and build the look up table, as shown in **Figure S5(d)**. The effective ALH from CLARS measurements is then retrieved by projecting on the lookup table. The geometric thickness of the aerosol layer can be derived from the correlation plot in **Figure 1(b)**. Assuming that the aerosol vertical distribution follows a normal distribution, we can reconstruct the aerosol vertical structure, as shown in **Figure 2(f)**, based on the retrieved total AOD, effective ALH, and the derived aerosol layer geometric thickness (see **Text S5** for details). It is evident that the retrieved profile reproduces the vertical structure of the measured profile very well.

(a) (b) (c)

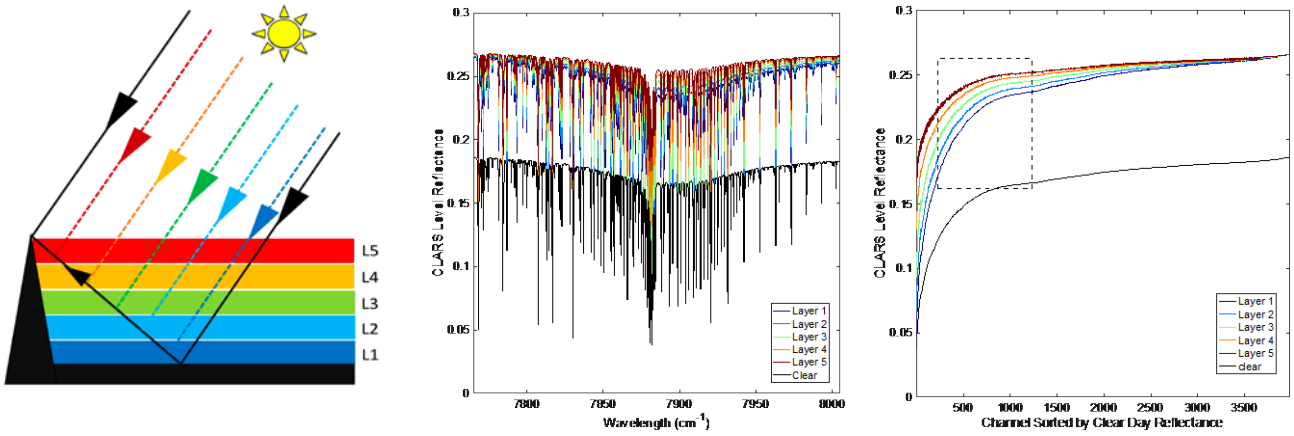

(d) (e) (f)

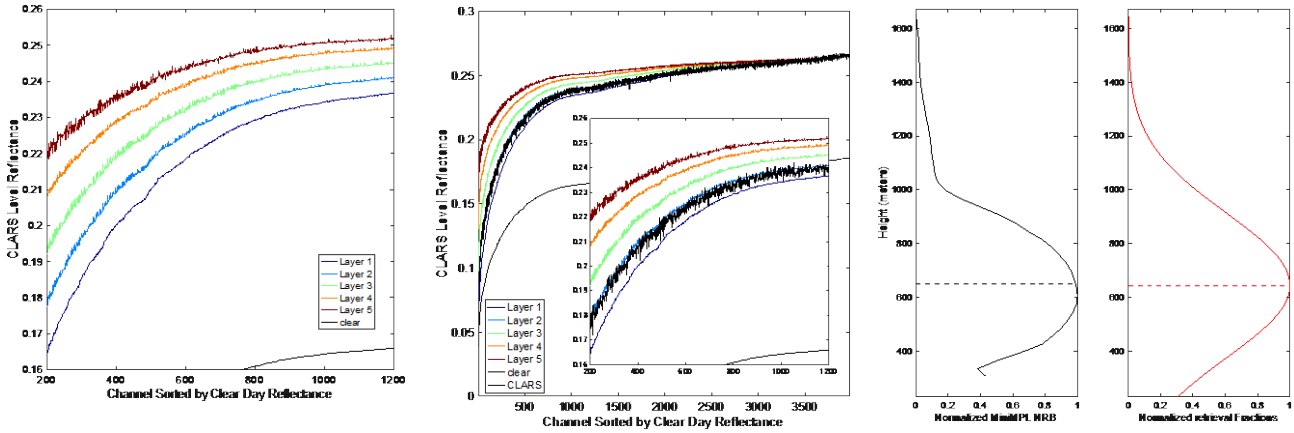

Figure 2. (a) Aerosol layer structures formulated in the RT model. Five aerosol layers are constructed by equally dividing the height from the surface (a.s.l. 292m for West Pasadena surface target) to the CLARS elevation (1673m). The layers are centered at 430, 706, 983, 1259, and 1535 meters, respectively, with layer vertical thickness of 276 meters. (b) Five aerosol layer scenarios simulated by adding the same amount of aerosol loading but in different layers. The simulated CLARS reflectance in the oxygen band is shown for the five scenarios (in blue to red from layer 1 to layer 5, respectively), as well as the clean scenario (in black). These simulations use the solar geometries at 14:00 on 17 September 2013, and collocated aerosol optical properties (SSA and phase function) from AERONET. The solar zenith angle is 46.56° and the aerosol scattering angle is 50.64°. (c) The simulated spectra from (b) sorted according to the reflectance value. The sorting order is obtained from the clear scenario spectra and then applied to all other scenarios. (d) Zoomed in plot of the rectangle shown in (c). (e) Same as (c) but overlaid with measured reflectance from CLARS. (f) Observed aerosol layer profile from MiniMPL and ALH (652 meters) in the left panel, and the retrieved profile and ALH (644 meters) in the right panel. The measured AOD (0.0257) and retrieved AOD (0.0279) at 1.27 μm are also indicated. The corresponding AOD at 0.5 um is about 0.10. The MiniMPL measurements are not available below 275 meters a.s.l., which is the height of the building where the instrument is located.

3.3 Assessment of retrieval accuracy

The retrieval accuracy of the proposed method is evaluated by applying the retrieval method to all available measurements with coincident CLARS, AERONET, and MiniMPL measurements from May 2013 to December 2014. Cases with high or low clouds are excluded using the oxygen ratio technique (Wong et al., 2015). For total AOD retrievals, 160 cases from collocated CLARS and AERONET measurements are available for this comparison, as shown in **Figure 3(a)**. The AOD ranges from 0 to 0.12 **(Figure S3)**. Aerosol optical properties from AERONET are used in

the RT model for the retrieval. The retrievals are significantly correlated with the AOD from AERONET (r^2 = 0.74; RMSE = 0.013). The total AOD retrieval has an error of 24.9% on average compared with AERONET data. Part of the variability may be due to the fact that the light paths for AERONET and CLARS are not the same. To compare the retrieved effective ALH with MiniMPL observations, data filtering is performed to ensure the validity of the measurements from AERONET and MiniMPL. First, cases with bad AOD retrieval (**Figure 3(a)**), i.e., retrieval error larger than 50% (about 10% of data involved), are not used. Second, we correlate the AERONET AOD with MiniMPL backscatter data, as shown in **Figure S4**. Data with difference (between AERONET and MiniMPL observations) larger than 1.5 standard deviations from the mean, as indicated by red, are not included. In general, these excluded cases are those days with large aerosol heterogeneity, such that the AERONET and MiniMPL data may not be representative of aerosol conditions within the CLARS light path. In total 53 cases are available from collocated CLARS, AERONET, and MiniMPL measurements. Three different levels of aerosol loading are plotted according to AOD. We found that retrievals for AOD larger than 0.02 are significantly correlated with the truth (r^2 = 0.57; RMSE = 67.01 m), as shown in **Figure 3(b)**. A much better performance can be found for cases with larger AOD because it provides higher aerosol scattering signal that can be captured by CLARS. When aerosol loading is weak, the aerosol scattering signal may be negligible compared to that from surface reflectance. Therefore, the retrieved effective ALH tends to be smaller than the truth and closer to the surface. The AOD of 0.02 at 1.27 um corresponds to about 0.085 at 0.50 um based on the averaged Angstrom coefficients that are related to the aerosol composition. The effective ALH retrieval has an error of 7.8% on average compared with the corresponding MiniMPL data. Overall, the proposed algorithm can accurately capture the variability of the total AOD and effective ALH in the PBL.

(a) (b)

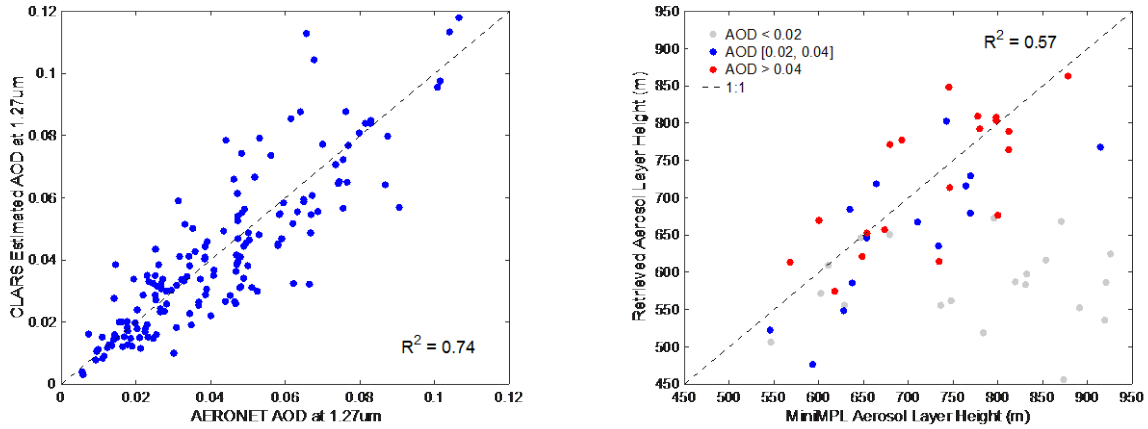

Figure 3. (a) Retrievals of total AOD at 14:00 from CLARS compared with corresponding AERONET-Caltech measurements. In total, 160 cases from collocated CLARS and AERONET measurements are available for this comparison. The retrievals are significantly correlated with the truth (r^2 = 0.74; RMSE = 0.013); (b) Retrievals of effective ALH from CLARS at 14:00 compared with the corresponding ALH derived from MiniMPL at Caltech. In total 53 cases are available from collocated CLARS, AERONET, and MiniMPL measurements. Three different levels of aerosol loading are plotted according to AOD; retrievals for AOD larger than 0.02 are significantly correlated with the truth (r^2 = 0.57; RMSE = 67.01 meters).

3.4 Impacts of SSA and phase function

The proposed profiling technique uses inversion products of SSA and phase function from AERONET in the study area and assumes that we have accurate estimates of these products, which may not always be the case. Here, we quantify the retrieval uncertainty on total AOD and effective ALH caused by errors in the SSA and phase function. For simplicity, the aerosol scattering in the model is assumed to follow the Henyey–Greenstein type phase function (Henyey and Greenstein, 1941), which depends solely on the asymmetry parameter. The results are shown in **Figure 4**. As the SSA increases, the aerosols appear brighter; therefore, the estimated total AOD is lower to match the observed radiance. On the other hand, the estimated

ALH increases because, for a given aerosol loading, a greater degree of scattering arises due to a shorter light path, as seen in the sensitivity study in **Figure 2(b)**. The effects of asymmetry parameter have a different pattern. As the asymmetry parameter increases, the phase function has a stronger peak in the forward direction (scattering angle less than 20 degrees) and a smaller fraction in the remaining scattering angles including the angle (50.64°) used in this simulation. In general, the error in total AOD retrieval is higher than that in ALH retrieval. As indicated by **Figure 3**, the RMSE in total AOD (0.013) is about 25% of the averaged total AOD (0.0541) in this simulation, while the RMSE in effective ALH (67 m) is about 10% of the true ALH (706 m). These error fractions are approximately comparable to the estimated errors due to a deviation of ±0.5σ in SSA and asymmetry parameter (**Figure 4**). A discussion on obtaining SSA and phase function from satellite retrievals and model simulations is provided in **Text S6**.

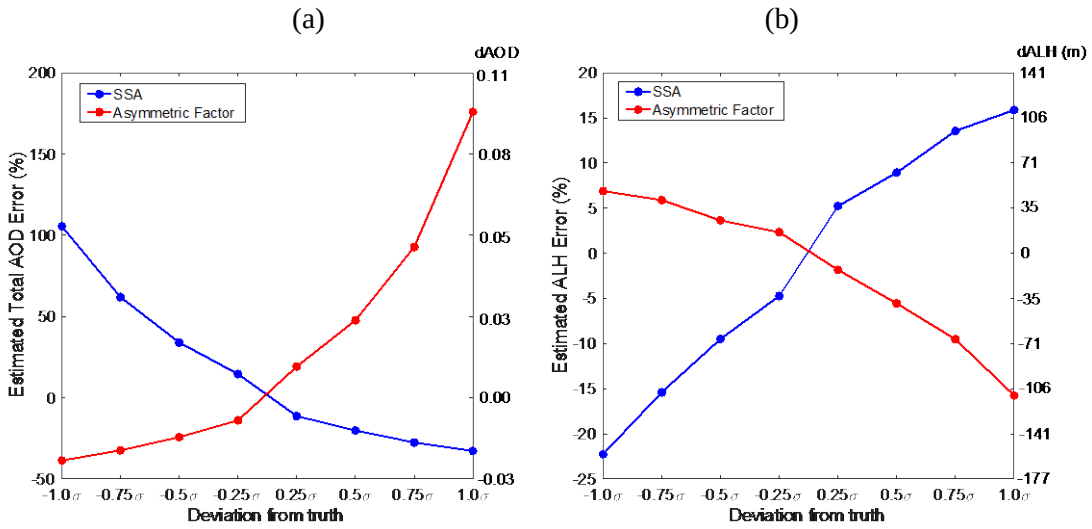

Figure 4. Uncertainty in total AOD and effective ALH retrievals from CLARS measurements caused by errors in input aerosol optical properties. The synthetic radiance observation is first generated using the same CLARS and solar geometries as in Figure 2, with aerosol in the middle layer (ALH=706 meters), and averaged total AOD (0.054), SSA (0.859), and asymmetry parameter (0.812) derived from long term AERONET measurements at Caltech. The

corresponding standard deviations (σ) for SSA (0.146) and asymmetry parameter (0.0877) are used as the estimation errors. The total AOD in (a) and ALH in (b) are then retrieved by applying the proposed method to the synthetic spectral data SSA or asymmetry parameter perturbed by a certain error (-1.0σ, -0.75σ, -0.5σ, -0.25σ, 0.25σ, 0.5σ, 0.75σ, 1.0σ). The estimation errors in total AOD and asymmetry parameter are calculated as the deviation (in percentage) from the known truth.

4. CONCLUSIONS

This work represents the first attempt to profile boundary layer aerosol vertical structure using hyperspectral remote sensing measurements. The proposed algorithm, which uses hyperspectral measurements in the 1.27 μm oxygen absorption band to retrieve the total AOD and the effective ALH, is applied to data from the CLARS-FTS instrument, located on a mountain top overlooking the LA basin. The effectiveness and accuracy of the retrievals are assessed by comparing with AOD from AERONET and backscatter profile from MiniMPL lidar measurements. The spectral sorting technique provides two advantages over a conventional fitting scheme: (1) information related to aerosol loading and its vertical structure can be extracted in a straightforward manner from the observed radiance; (2) the spectral region(s) with the largest sensitivity to arbitrary geophysical retrieval parameters (total AOD and ALH in this study) can be identified. The proposed retrieval algorithm to constrain aerosol vertical distribution will potentially help quantify the aerosol direct radiative forcing and reduce bias in greenhouse gas retrievals from space due to uncertainty caused by aerosol scattering.

The algorithm developed in this study has two implications for analyzing space-borne observations, such as hyperspectral O_2 A-band measurements from the OCO-2 (Crisp et al., 2012) and the upcoming OCO-3 (Eldering et al., 2013) missions. First, accuracy of ALH retrieval shows a certain dependence on SSA and phase function, whose retrieval accuracies can be further improved by combining hyperspectral oxygen absorption and polarimetric measurements

in a broad spectral range (e.g. UV-NIR of AirMSPI (Diner et al. 2013, Xu et al., 2017) and UV-SWIR of RSP (Cairns et al. 1999; Wu et al. 2015)) to simultaneously determine aerosol profile and microphysical properties as well as surface reflection. Moreover, polarization measurements may also improve the aerosol layer detection over bright surfaces (see the discussion on surface albedo in **Text S7**). Second, a larger viewing angle off-nadir measurement provides more aerosol information, e.g., OCO-3 off-nadir measurements with the urban target mode. In the near future, CLARS-FTS will be upgraded to include measurements in the O_2 A-band at 0.76 μm. The O_2 A-band is more sensitive to scattering from fine mode aerosols while the O_2 $^1\Delta$ band at 1.27 μm is more sensitive to scattering from coarse mode aerosols. A combination of these spectral regions may help to distinguish the profiles of fine and coarse mode aerosols.

Acknowledgement

We thank Jack Margolis, Chao Liu, Yuan Wang, Siteng Fan, Sunitі Sanghavi, Mike Gunson and Annmarie Eldering for stimulating discussions. VN acknowledges support from the NASA Earth Science US Participating Investigator program (solicitation NNH16ZDA001N-ESUSPI). FX acknowledges support from NASA Remote Sensing Theory program under grant #14-RST14-0100. We are also thankful for the support from the Jet Propulsion Laboratory Research and Technology Development Program. Part of the research in this study was performed at the Jet Propulsion Laboratory, California Institute of Technology, under a contract with the National Aeronautics and Space Administration. The CLARS project receives support from the California Air Resources Board and the NIST GHG and Climate Science Program. The MiniMPL was supported by the KISS Program at Caltech; data are available from the NASA Megacity project data portal: https://megacities.jpl.nasa.gov/portal/. AERONET data for the Caltech site are available from https://aeronet.gsfc.nasa.gov/new_web/photo_db_v3/CalTech.html. We also thank Jochen Stutz from UCLA and his staff for their effort in establishing and maintaining the AERONET Caltech site. CLARS-FTS data are available from the authors upon request and part of the data are available from the NASA Megacities Project at https://megacities.jpl.nasa.gov. We are grateful to the two anonymous reviewers whose comments helped improve the paper.

References:

Bond, T. C., Doherty, S.J., Fahey, D.W., Forster, P.M., Berntsen, T., DeAngelo, B.J., et al. (2013). Bounding the role of black carbon in the climate system: A scientific assessment. *J. Geophys. Res.*, 118(11), 5380–5552.

Butz, A., Hasekamp, O. P., Frankenberg, C., and Aben, I. (2009). Retrievals of Atmospheric CO_2 from Simulated Space-Borne Measurements of Backscattered Near-Infrared Sunlight: Accounting for Aerosol Effects. *Appl. Opt.*, 48(18), 3322–3336. doi:10.1364/AO.48.003322.

Cairns, B., Russell, E.E. and Travis, L.D. (1999). Research scanning polarimeter: calibration and ground-based measurements. In *Polarization: Measurement, Analysis, and Remote Sensing* II (Vol. 3754, pp. 186–197). International Society for Optics and Photonics.

Colosimo, S. F., Natraj, V., Sander, S. P., and Stutz, J. (2016). A sensitivity study on the retrieval of aerosol vertical profiles using the oxygen A-band, *Atmos. Meas. Tech.*, 9, 1889–1905. doi:10.5194/amt-9-1889-2016.

Crisp, D., Fisher, B. M., O'Dell, C., Frankenberg, C., Basilio, R., Bösch, H., et al. (2012). The ACOS CO_2 retrieval algorithm – Part II: Global XCO_2 data characterization. *Atmos. Meas. Tech.*, 5, 687–707. doi:10.5194/amt-5-687-2012.

Davis, A. B., Kalashnikova, O. V., and Diner, D. J. (2017). Aerosol Layer Height Over Water from O_2 A-band: Mono-Angle Hyperspectral and/or Bi-spectral Multi-Angle Observations. *Preprint*, doi:10.20944/preprints201710.0055.v1.

Diner, D. J., Beckert, J. C., Reilly, T. H., Bruegge, C. J., Conel, J. E., Kahn, R. A. (1998). Multi-angle Imaging SpectroRadiometer (MISR) instrument description and experiment overview. *IEEE Trans. Geosci. Remote Sens.*, 36(4), 1072–1087.

Diner, D. J., Braswell, B. H., Davies, R., Gobron, N., Hu, J., Jin, Y., et al. (2005). The value of multiangle measurements for retrieving structurally and radiatively consistent properties of clouds, aerosols, and surfaces. *Remote Sens. Environ.*, *97*(4), 495–518.

Ding, S., Wang, J. and Xu, X. (2016). Polarimetric remote sensing in oxygen A and B bands: Sensitivity study and information content analysis for vertical profile of aerosols. *Atmos. Meas. Tech.*, 9(5), 2077–2092. doi: 10.5194/amt-9-2077-2016.

Dubuisson, P., Frouin, R., Dessailly, D., Duforêt, L., Léon, J.-F., Voss, K., et al. (2009). Estimating the altitude of aerosol plumes over the ocean from reflectance ratio measurements in the O_2 A-band. *Remote Sens. Environ.*, 113(9), 1899–1911.

Eldering, A., Kaki, S., Crisp, D. and Gunson, M.R. (2013). The OCO-3 mission. In AGU Fall Meeting Abstracts, American Geophysical Union, Fall Meeting 2013, San Francisco.

Frankenberg, C., Butz, A. and Toon, G.C. (2011). Disentangling chlorophyll fluorescence from atmospheric scattering effects in O_2 A‐band spectra of reflected sun‐light. *Geophys. Res. Lett.*, 38(3).

Fu, D., Pongetti, T. J., Blavier, J.-F. L., Crawford, T. J., Manatt, K. S., Toon, G. C., et al. (2014). Near-infrared remote sensing of Los Angeles trace gas distributions from a mountaintop site. *Atmos. Meas. Tech.*, 7, 713–729

Gabella, M., Kisselev, V., Perona, G. (1999). Retrieval of aerosol profile variations from reflected radiation in the oxygen absorption A band. *Appl. Opt.*, 38, 3190–3195. doi:10.1364/AO.38.003190.

Geddes, A. and Bösch, H. (2015). Tropospheric aerosol profile information from high-resolution oxygen A-band measurements from space. *Atmos. Meas. Tech.*, 8(2), 859–874. doi:10.5194/amt-8-859-2015.

Heidinger, A., and Stephens, G.L. (2000). Molecular line absorption in a scattering atmosphere, part II: application to remote sensing in the O_2 A-band. *J. Atmos. Sci.*, 57, 1615–1634. doi:10.1175/1520-0469.

Holben, B. N., Eck, T. F., Slutsker, I., Tanre, D., Buis, J. P., and Setzer, A. (1998). AERONET – A federated instrument network and data archive for aerosol characterization, *Remote Sens. Environ.*, 66, 1–16, 1998.

Hollstein, A. and Fischer, J. (2014). Retrieving aerosol height from the oxygen A band: a fast forward operator and sensitivity study concerning spectral resolution, instrumental noise, and surface inhomogeneity. *Atmos. Meas. Tech.*, 7(5), 1429–1441.

Hou, W., Wang, J., Xu, X., and Reid, J.S. (2017). An algorithm for hyperspectral remote sensing of aerosols: 2. Information content analysis for aerosol parameters and principal components of surface spectra. *J. Quant. Spectrosc. Radiat. Transfer*, 192, 14–29.

Irion, F.W., Gunson, M.R., Toon, G.C., Chang, A.Y., Eldering, A., Mahieu, E., et al. (2002). Atmospheric Trace Molecule Spectroscopy (ATMOS) Experiment Version 3 data retrievals. *Appl. Opt.*, 41(33), 6968–6979.

IPCC (2013). Climate Change 2013: The Physical Science Basis. Contribution of Working Group I to the Fifth Assessment Report of the Intergovernmental Panel on Climate Change [Stocker, T.F., D. Qin, G.-K. Plattner, M. Tignor, S.K. Allen, J. Boschung, A. Nauels, Y. Xia, V. Bex and P.M. Midgley (eds.)]. Cambridge University Press, Cambridge, United Kingdom and New York, NY, USA, doi:10.1017/CBO9781107415324.

Jethva, H., Torres, O. and Ahn, C. (2014). Global assessment of OMI aerosol single-scattering albedo using ground-based AERONET inversion. *J. Geophys. Res.*, *119*(14), doi:10.1002/2014JD021672.

Kahn, R. A., Garay, M. J., Nelson, D. L., Yau, K. K., Bull, M. A., Gaitley, B. J., et al. (2007). Satellite-Derived Aerosol Optical Depth over Dark Water from MISR and MODIS: Comparisons with AERONET and Implications for Climatological Studies. *J. Geophys. Res.*, 112(18), doi:10.1029/2006JD008175.

Kalnay, E., Kanamitsu, M., Kistler, R., Collins, W., Deaven, D., Gandin, L., et al. (1996). The NCEP/NCAR 40-year reanalysis project, *B. Am. Meteorol. Soc.*, 77, 437–471.

Kinne, S., Lohmann, U., Feichter, J., Schulz, M., Timmreck, C., Ghan, S., et al. (2003). Monthly averages of aerosol properties: A global comparison among models, satellite data, and AERONET ground data. *J. Geophys. Res.*, *108*(D20), doi:10.1029/2001JD001253.

Koffi, B., Schulz, M., Bréon, F. M., Griesfeller, J., Winker, D., Balkanski, Y., et al. (2012). Application of the CALIOP layer product to evaluate the vertical distribution of aerosols estimated by global models: AeroCom phase I results. *J. Geophys. Res.*, 117, D10201, doi:10.1029/2011JD016858.

Kuang, Z. M., Margolis, J., Toon, G., Crisp, D., and Yung, Y. L. (2002). Spaceborne Measurements of Atmospheric CO_2 by High-resolution NIR Spectrometry of Reflected Sunlight: An Introductory Study. *Geophys. Res. Lett.*, 29(15), 1716, doi:10.1029/2001GL014298.

Liu, Y., and Diner, D. J. (2017). Multi-angle imager for aerosols: a satellite investigation to benefit public health, *Public Health Rep.*, 132, 14–17.

O'Brien, D.M., and Mitchell, R.M. (1992). Error estimates for retrieval of cloud-top pressure using absorption in the A-Band of oxygen. *J. Appl. Meteorol.*, 31, 1179–1192.

O'Dell, C. W., Connor, B., Bösch, H., O'Brien, D., Frankenberg, C., Castano, R., et al. (2012). The ACOS CO_2 retrieval algorithm – Part 1: Description and validation against synthetic observations. *Atmos. Meas. Tech.*, 5, 99–121, doi:10.5194/amt-5-99-2012.

Richardson, M., McDuffie, J., Stephens, G. L., Cronk, H. Q., and Taylor, T. E. (2017). The OCO-2 oxygen A-band response to liquid marine cloud properties from CALIPSO and MODIS, *J. Geophys. Res.*, 122, 8255–8275, doi:10.1002/2017JD026561.

Sanghavi, S., Martonchik, J. V., Landgraf, J., and Platt, U. (2012). Retrieval of aerosol optical depth and vertical distribution using O_2 A- and B-band SCIAMACHY observations over Kanpur: A case study. *Atmos. Meas. Tech.*, 5(5), 1099–1119.

Seinfeld, J. and Pandis, S. (2006). Atmospheric chemistry and physics: from air pollution to climate change. Wiley, Inc., New Jersey, USA, p. 1224

Sen, B., Toon, G. C., Blavier, J.-F., Fleming, E. L., and Jackman, C. H. (1996). Balloon-borne observations of mid-latitude fluorine abundance. *J. Geophys. Res.*, 101, 9045–9054.

Spurr, R. J. D., and Natraj, V. (2011). A linearized 2-stream radiative transfer code for fast approximation of multiple-scatter fields, *J. Quant. Spectrosc. Radiat. Transfer*, 112(16), 2630–2637.

Timofeyev, Y. M., Vasilyev, A. V., and Rozanov, V. V. (1995). Information content of the spectral measurements of the 0.76 μm O_2 outgoing radiation with respect to the vertical aerosol optical properties. *Adv. Space Res.*, 16, 91–94.

Thompson, J. E., Hayes, P. L., Jimenez, J. L., Adachi, K., Zhang, X., and Liu, J. (2012). Aerosol optical properties at Pasadena, CA during CalNex 2010. *Atmos. Environ.*, 55, 190–200.

Wang, J., Xu, X., Ding, S., Zeng, J., Spurr, R., Liu, X., et al. (2014). A numerical testbed for remote sensing of aerosols, and its demonstration for evaluating retrieval synergy from a geostationary satellite constellation of GEO-CAPE and GOES-R. *J. Quant. Spectrosc. Radiat. Transfer*, 146, 510–528.

Ware, J., Kort, E.A., DeCola, P., and Duren, R. (2016). Aerosol lidar observations of atmospheric mixing in Los Angeles: Climatology and implications for greenhouse gas observations. *J. Geophys. Res. Atmos.*, 121(16), 9862–9878.

Winker, D. M., Vaughan, M. A., Omar, A., Hu, Y., Powell, K. A., Liu, Z., et al. (2009). Overview of the CALIPSO Mission and CALIOP Data Processing Algorithms, *J. Atmos. Ocean. Tech.*, 26(11), 2310–2323.

Wong, K. W., Fu, D., Pongetti, T. J., Newman, S., Kort, E. A., Duren, R., et al. (2015). Mapping CH_4 : CO_2 ratios in Los Angeles with CLARS-FTS from Mount Wilson, California, *Atmos. Chem. Phys.*, 15, 241–252, doi:10.5194/acp-15-241-2015, 2015.

Wong, C. K., Pongetti, T. J., Oda, T., Rao, P., Gurney, K. R., Newman, S., et al. (2016). Monthly trends of methane emissions in Los Angeles from 2011 to 2015 inferred by CLARS-FTS observations, *Atmos. Chem. Phys.*, 16, 13121–13130, doi:10.5194/acp-16-13121-2016.

Wu, L., Hasekamp, O., Van Diedenhoven, B. and Cairns, B. (2015). Aerosol retrieval from multiangle, multispectral photopolarimetric measurements: importance of spectral range and angular resolution. *Atmos. Meas. Tech.*, 8, 2625–2638.

Wunch, D., Toon, G. C., Blavier, J.-F. L., Washenfelder, R. A., Notholt, J., Connor, B. J., et al. (2011). The total carbon column observing network, *Philos. Trans. A Math. Phys. Eng. Sci.*, 369(1943), 2087–2112, doi:10.1098/rsta.2010.0240.

Xi, X., Natraj, V., Shia, R. L., Luo, M., Zhang, Q., Newman, S., Sander, S. P., and Yung, Y. L. (2015). Simulated retrievals for the remote sensing of CO_2, CH_4, CO, and H_2O from geostationary orbit, *Atmos. Meas. Tech.*, 8, 4817–4830, doi:10.5194/amt-8-4817-2015.

Xu, F., van Harten, G., Diner, D. J., Kalashnikova, O. V., Seidel, F. C., Bruegge, C. J., and Dubovik, O. (2017). Coupled retrieval of aerosol properties and land surface reflection using the Airborne Multiangle SpectroPolarimetric Imager (AirMSPI), *J. Geophys. Res., Atmos.*, 122, 7004–7026.

Xu, X., Wang, J., Wang, Y., Zeng, J., Torres, O., Yang, Y., Marshak, A., Reid, J., and Miller S. (2017). Passive remote sensing of altitude and optical depth of dust plumes using the oxygen A and B bands: First results from EPIC/DSCOVR at Lagrange-1 point. *Geophys. Res. Lett.*, 44, 7544–7554, doi:10.1002/ 2017GL073939.

Yamamoto, G., and Wark, D.Q. (1961). Discussion of the letter by R.A. Hanel, Determination of cloud altitude from a satellite. *J. Geophys. Res.*, 66, 3596.

Zarzycki, C. M., and Bond, T. C. (2010). How much can the vertical distribution of black carbon affect its global direct radiative forcing? *Geophys. Res. Lett.*, 37, L20807.

Zeng, Z.-C., Zhang, Q., Natraj, V., Margolis, J. S., Shia, R.-L., Newman, S., et al. (2017). Aerosol scattering effects on water vapor retrievals over the Los Angeles Basin. *Atmos. Chem. Phys.*, 17, 2495–2508.

Zhang, Q., Natraj, V., Li, K.-F., Shia, R.-L., Fu, D., Pongetti, T. J., et al. (2015). Accounting for aerosol scattering in the CLARS retrieval of column averaged CO_2 mixing ratios. *J. Geophys. Res.-Atmos.*, 120, 7205–7218, doi:10.1002/2015JD023499.

Zhang, Q., Shia, R.-L., Sander, S. P., and Yung, Y. L. (2016). XCO_2 retrieval error over deserts near critical surface albedo, *Earth Space Sci.*, 2, 1–10, doi:10.1002/2015EA000143.

(a)

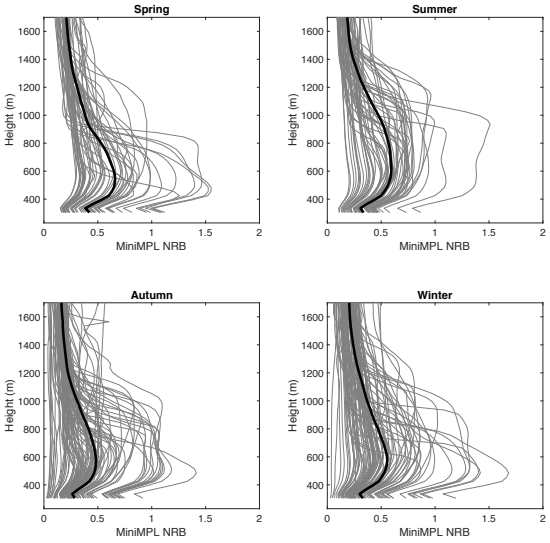

(b)

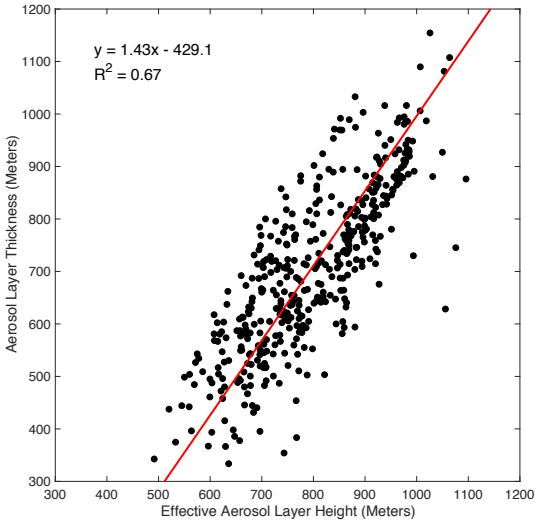

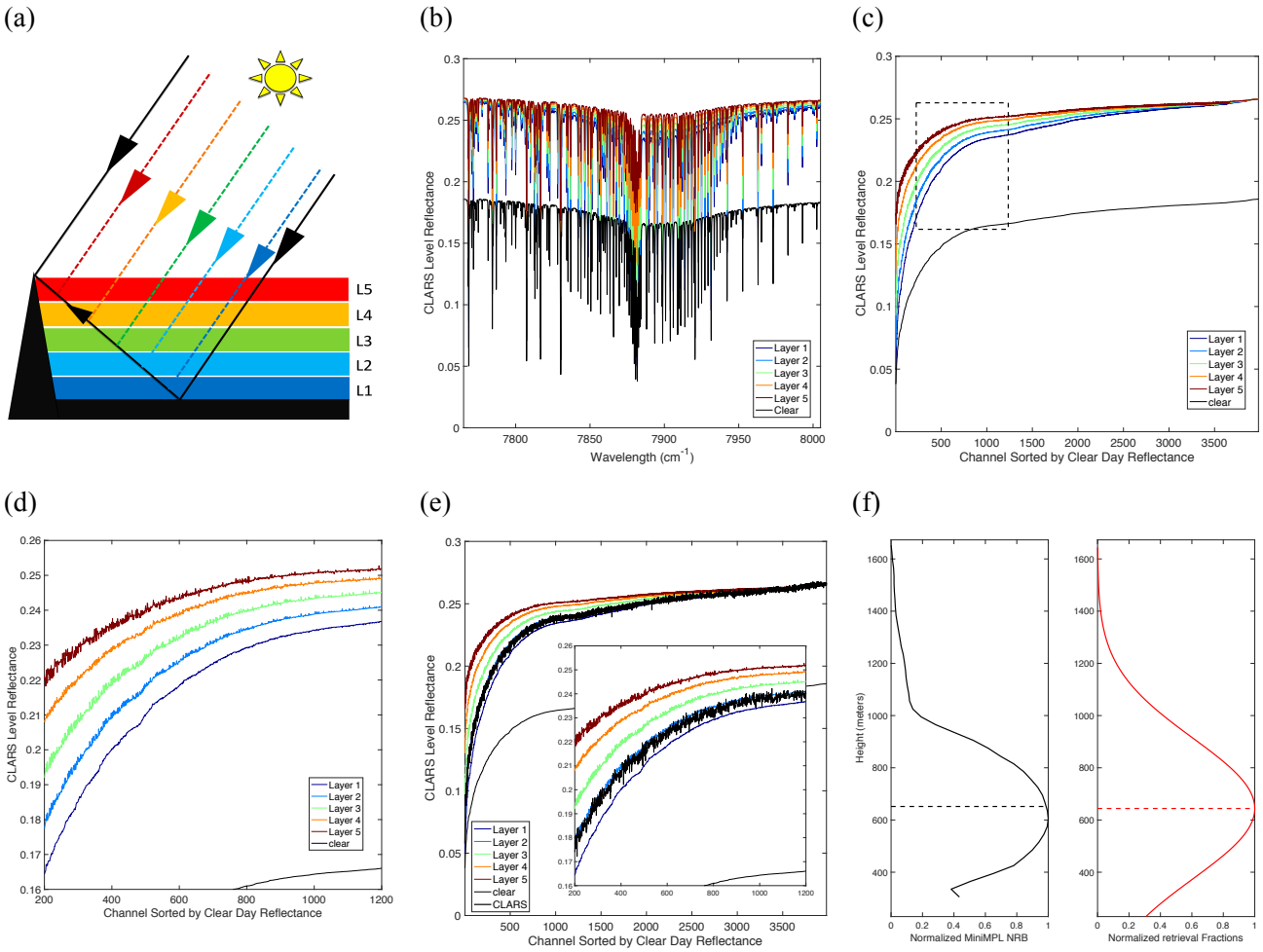

(a)

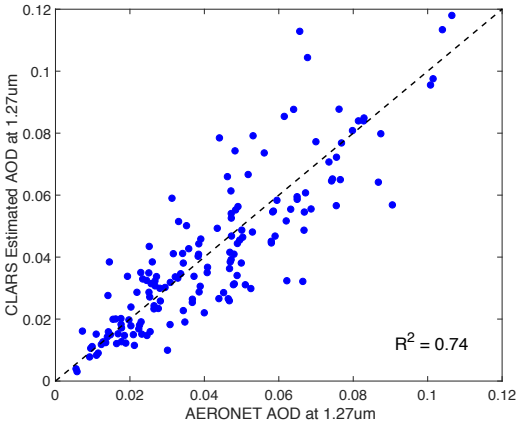

(b)

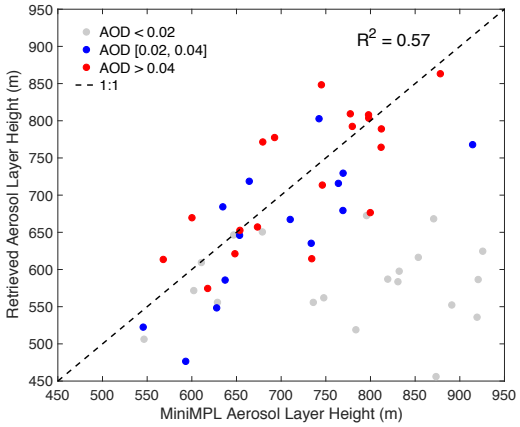

(a)

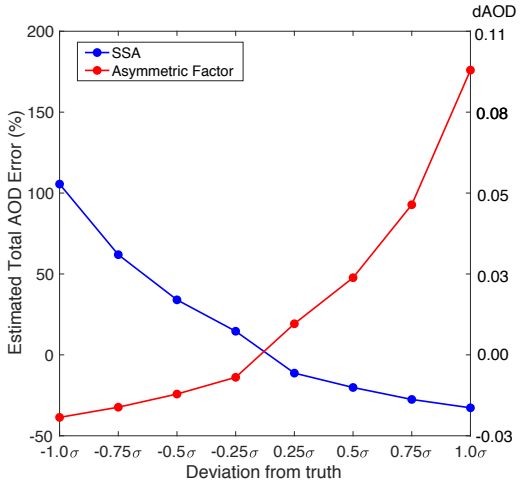

(b)